Iranian Journal of Materials Forming 9 (4) (2022) 44-55

Online ISSN: 2383-0042

IJMF

Iranian Journal of Materials Forming

Journal Homepage: http://ijmf.shirazu.ac.ir

Research Article

Effect of Welding Processes on Texture and Anisotropy of HSLA Steel Sheet

M. Golmohammadi and M. Aghaie-Khafri*

Faculty of Materials Science and Engineering, K.N. Toosi University of Technology, Postal Code: 1999143344, Tehran, Iran

ARTICLE INFO

Article history:

Received 16 October 2022
Reviewed 20 November 2022
Revised 5 December 2022
Accepted 12 December 2022

Keywords:

HSLA steel
Anisotropy
Macro texture
Mechanical properties
Welding

Please cite this article as:

M. Golmohammadi, M. Aghaie-Khafri, Effect of welding processes on texture and anisotropy of HSLA steel sheet, *Iranian Journal of Materials Forming*, 9(4) (2022) 44-55.

ABSTRACT

In the present investigation, the effect of welding processes on the microstructure, crystallographic texture, mechanical properties, and anisotropy of weldment joints of a high strength low alloy steel (HSLA) was studied. The main goal of this research is to establish the relationship between microstructure, texture evolutions, and mechanical properties of the weldments. GTAW and SMAW welding processes were conducted, and macro texture of samples was investigated with the X-ray diffraction technique. Mechanical properties were evaluated by using the uniaxial tensile test in three directions of 0, 45, and 90° to the weld line and a micro hardness test. Preferred orientation in the weldment develops in different welding processes based on the initial base metal texture. The texture of the base metal consisted of γ-fiber, α-fiber, G {110} <001>, and R-Cube {001} <110> main components that evolves during the welding processes. Weakening of the γ-fiber texture component results in a significant reduction in the mechanical properties of the weldments. Moreover, the percentage of the γ-fiber component in the GTAW sample is greater than the SMAW sample, which results in superior mechanical properties.

© Shiraz University, Shiraz, Iran, 2022

1. Introduction

The industry's demand for low alloy steels and in particular the need of materials with high strength-to-weight ratio in strategic industries [1], makes high strength low alloy (HSLA) steels a popular topic for research. This group of steels is classified as heat-treated low-alloy steels according to their percentage of elements. HSLA steels are actually carbon steels in which alloying elements are added in small quantities to improve various properties such as hardness, strength, and corrosion resistance [2, 3]. High corrosion resistance, strength, excellent formability, toughness, impact resistance (especially at low temperatures), as well as proper weldability of HSLA steels bring them many engineering structural applications [4, 5] in various industries such as oil and gas transmission pipelines, oil rigs, tanks, automotive industry [6, 7], bridges and civil structures, the hulls of naval ships and submarines, and aerospace industries [8-13].

* Corresponding author
E-mail address: maghaei@kntu.ac.ir (M. Aghaie-Khafri)
https://doi.org/10.22099/IJMF.2023.44992.1240

Published by Shiraz University. This is an open access article under the CC BY-NC-ND license (http://creativecommons.org/licenses/by-nc-nd/4.0/).

Despite the good weldability of HSLA steels, welding often destroys the weldment microstructure. When HSLA steel is welded, non-uniform heating and cooling in the weld metal and base metal generates heat affected zone (HAZ), cold crack susceptibility, and residual stress in weldments [14, 15]. This issue has a great impact on the mechanical properties of welded joints [16]. Many studies have shown a decrease of mechanical properties in the welding section in comparison with the base metal [17-19]. Welding parameters such as current intensity, voltage, size, type of the filler metal, welding speed, and the welding method significantly affect the microstructure, crystallographic texture, and mechanical properties of the welding zones [20-22]. Therefore, in order to obtain superior welding quality as well as optimal mechanical properties of the weld joint, welding parameters must be properly adjusted.

Talabi et al. [22] investigated the effect of manual electrode welding parameters on the mechanical properties of 10 mm thick low carbon steel sheets. They considered current intensity, arc voltage, welding speed, and electrode diameter as welding variables. Results showed that these parameters have a direct effect on the mechanical properties of the welded joints. Increasing the voltage and current intensity decreased the yield strength, tensile strength, and the impact resistance. Furthermore, by increasing the welding speed, the hardness of the welding section was increased.

Simhachalam et al. [23] investigated the effect of current intensity, shielding gas flow, and diameter of the filler metal on the mechanical properties of SS304 steel. They observed that the welding current intensity has a significant effect on the mechanical properties.

Lal et al. [24] investigated the homogeneous and heterogeneous tungsten inert gas (TIG) welding joints of the austenitic stainless steels SS304 and SS316. The highest tensile strength and toughness were observed in SS304-SS304 joint, and the highest hardness was achieved for SS304-SS316.

Yan et al. [25] investigated the microstructure and mechanical properties of the joints of the SS304 stainless steel welded with TIG, laser, and TIG-laser combination methods. Their results showed that the weld obtained from the laser welding has the highest tensile strength and the smallest size of dendritic grains formed in the welded zone. Moreover, the joint welded by the TIG method had the largest dendrite and the lowest tensile strength. They concluded that the laser welding process and the TIG-laser combination welding have better mechanical properties.

The study on the effect of TIG welding parameters on the microstructure, texture, and mechanical properties of AISI SS304 steel by Shaha et al. [26] showed that increasing the welding speed and intensity can increase the mechanical properties of the weld metal as a result of microstructure and texture evolutions.

Most of the research on the effect of welding parameters has focused on the microstructure and mechanical properties of the welding areas, and very little information is available on the texture characterizations of weldments [17, 26-28]. However, in welding processes the properties of the weld joints such as strength, toughness, ductility, and corrosion resistance can be dependent on the crystallographic texture [29]. Therefore, the study of the effect of welding parameters on the texture evolutions is essential for the development of welding processes.

The main goal of this study is to investigate and compare the effect of gas tungsten arc welding (GTAW) and submerged arc welding (SMAW) processes of HSLA steel on the crystallographic texture evolutions, microstructure, mechanical properties, and anisotropy of weldments.

2. Experimental Procedure

In the present study, HSLA steel API 5L X52 was used as the base metal. The result of chemical composition analysis is presented in Table 1. To perform the welding process, HSLA specimens were cut from 10 mm thick sheets of 220×100 mm [30]. Fig. 1 shows a schematic of the assembly and preparation of the sheets.

Specimens were welded by two methods of GTAW and SMAW. ER70S-3 and E7016-1 filler metals were used for the GTAW and SMAW welding, respectively.

Table 2 shows the chemical composition of electrodes by weight percentage. The GTAW samples were welded by AC/DC 3500W GTAW machine with DC current. Welding conditions and parameters in both GTAW and SMAW are presented in Table 3.

Multi-pass welding was performed from both sides of the specimens. When the root layers on both sides had finished being weld, the second layer and the supplementary layers were immediately welded. In order to prevent the welding layers from cooling down and the local separation between the layers, the welding of all the passes was immediately performed with no interruption. Thus, there was no need to apply heating between the passes.

To maintain consistency with the terms commonly used for welding processes, the main directions of "rolling direction", normal direction", and "welding direction" are referred to hereafter as RD, ND, and WD.

Specimens for metallography, including weld metal, base metal, and heat affected zones, were cut according to Fig. 2. Metallography of specimens were conducted by grinding up to 5000 emery paper and polishing with diamond paste (2 µm particles size). The specimens were etched with Nital 2% (98 ml C_2H_5OH+2 ml HNO_3), and microstructure of specimens were evaluated by optical microscopy.

Concerning texture evaluation, base metal and welding specimens were cut perpendicular to the direction of welding (ND-RD cross section). Subsequently, grinding and polishing were carefully performed. An X-ray texture angle detector based on Schulz reflection geometry, Philips X'Pert X-ray diffractometer, was utilized using Cu-k_α radiation. The polar images of the (110) plane were calculated using the High Score X'Pert software.

The mechanical properties of the welded joints were measured by the uniaxial tensile and Vickers hardness tests. Hardness measurements were performed across the weld section of the specimens on the ND-RD surface of metallographic specimens (Fig. 2) according to the ASTM E 384-17, using Vickers micro-hardness tester with a load of 300 gf and a loading time of 10 s. Vickers hardness profile was measured following etching metallographic

Table 1. Chemical composition of API 5L X52 (in wt.%)

Composition	wt.%
C	0.06
Si	0.14
Mn	1.02
P	0.01
Cr	0.02
V	0.01
Mo	0.1
Ni	0.02
CE	0.26
Cu	0.01
Ti	0.01
Nb	0.04
Al	0.03
Fe	Bal.

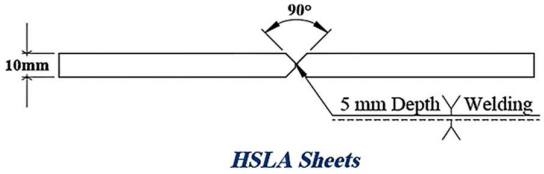

Fig. 1. Schematic of samples preparation for butt-weld welding.

Table 2. Chemical composition of ER70S-3 and E7016-1 electrodes [25]

Welding process	Filler metal	C (wt.%)	Si (wt.%)	Mn (wt.%)
GTAW /TIG	ER70S-3	0.1	0.6	1.2
SMAW	E7016-1	0.07	0.5	1.1

Table 3. GTAW and SMAW welding parameters

Parameter	SMAW	GTAW
Filler metal (electrode)	E7016-1	ER70S-3
Filler diameter (mm)	2.5	2.4
Number of passes	8	8
Current (A)	110	120
Voltage (V)	25	30
Welding speed (mm/min)	70	120
Argon gas flow rate (L/min)	-	12

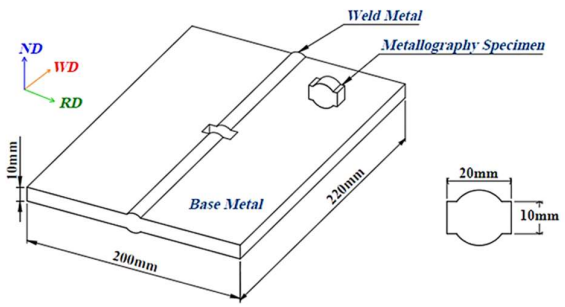

Fig. 2. Schematic of preparation and dimensions of metallographic specimens.

specimens and microscopic examinations. An average of 13 points in the RD direction and 5 points in the ND direction of the weld joint were measured.

Tensile strength and the percentage of the elongation of the specimens were measured using the uniaxial tensile test. The tensile test was performed on different specimens in three directions with angles of 0, 45, and 90° to the weld. Sub-size specimens for tensile test are shown in Fig. 3 [31]. It is worth mentioning that the welding specimens were cut in such a way that the welding line was exactly in the middle of the specimens, as shown in Fig. 4. Tensile test was performed by means of INSTRON-8502 at a cross-head speed of 2 mm/min.

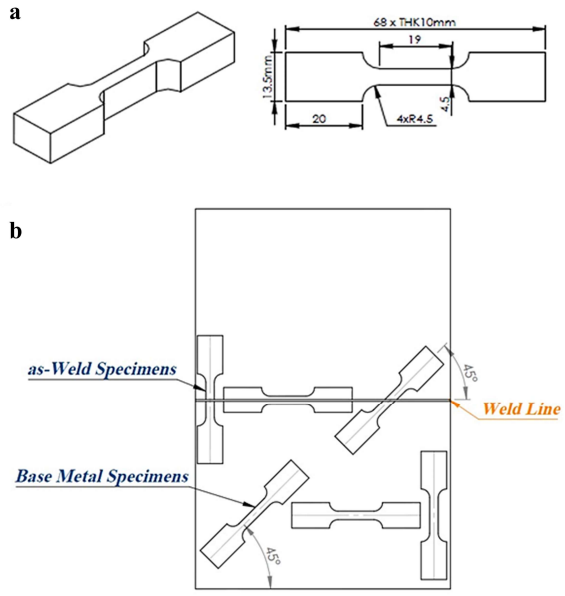

Fig. 3. Schematic of (a) the sub-size specimens used for the tensile test, (b) position and angle of the welded specimens and the cut base metal for the tensile test relative to the weld line.

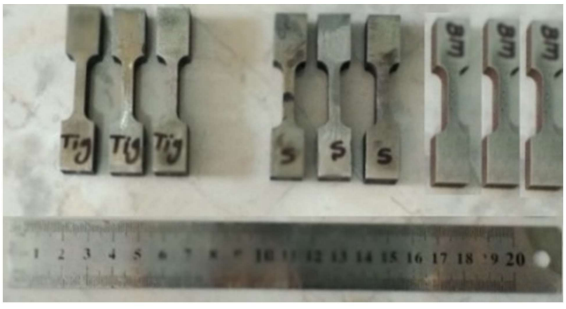

Fig. 4. HSLA welding specimens after welding processes.

3. Results and Discussion

3.1. Optical microstructural analysis

Welded specimens have three distinct regions of base metal, heat-affected zone (HAZ), and weld zone. Microstructure of HSLA specimens is shown in Fig. 5. As can be seen, Fig. 5(a) and 5(b) show the base metal microstructure before welding and consist of alpha ferrite with pearlite islands.

Fig. 5(c) and 5(d) show the intersection of the penetration zone and the heat affected zone of the GTAW specimen. It can be observed that the microstructure of the weld penetration zone includes acicular ferrite, bainite, and Widmanstätten ferrite. In the welding area, acicular ferrite is more than in the heat affected area. Acicular ferrite shows good resistance to the crack propagation and increases the impact toughness [27]. The heat-affected zone consisted of coarser granulation (growth of primary grains due to the increase

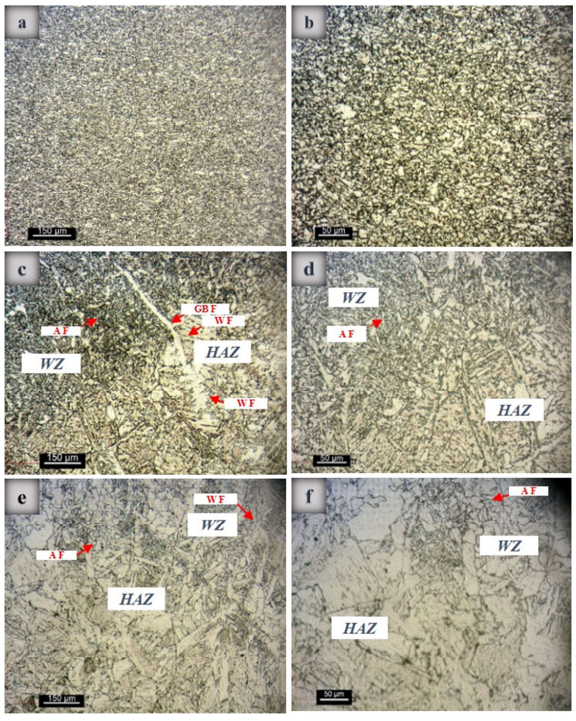

Fig. 5. Microstructure of welding zones of HSLA specimens, (a) and (b) base metal, (c) and (d) weld metal (WM) joint and heat affected area (HAZ) of GTAW welding specimen, (e) and (f) weld metal joint and heat affected area of the SMAW welding specimen, where acicular ferrite (AF), Widmanstätten ferrite (WF), and grain boundary ferrite (GBF) are indicated by red arrows.

in the welding temperature) and a cohesive structure with a higher percentage of Widmanstätten ferrite and dendritic grains. Small amounts of polygonal ferrite can also be seen in both areas.

Figs. 5(e) and 5(f) show the SMAW welding section and the heat affected area, which include acicular ferrite, Widmanstätten ferrite, small amounts of the boundary ferrite, and polygonal ferrite. It is clear that the percentage of the acicular ferrite is lower than the welding area of the specimen. Although the generation of the acicular ferrite improves the tensile strength and toughness, the presence of grain ferrite and Widmanstätten improves the brittleness and reduces the toughness of the weld [32]. In addition, the HAZ consisted of smaller percentages of the acicular ferrite and larger grains in comparison with the diffusion zone of the weld.

The heat affected zone of the SMAW welding specimen has a larger grain size than the GTAW specimen due to the high inlet temperature during the welding and the slower solidification due to the presence of the slag. It should be noted that if the solidification rate is increased, the Widmanstätten grain boundary ferrite is formed, and further increase in the solidification speed is pertained to the formation of the needle ferrites. Therefore, due to the rapid solidification, more needle ferrite is produced [28]. The presence of the needle ferrite in the weld metal is associated with better mechanical properties such as strength, ductility, resistance to the crack propagation, and greater impact resistance [33-36].

3.2. Texture analysis

Macroscopic texture evolutions of HSLA specimens for different welding processes were studied by means of XRD. In BCC metals, most of the pole figures with the highest intensity are presented in the {110} plane [23, 24]. Therefore, pole figure analysis of HSLA specimens was performed on the (110) plane. The ideal pole figures of the (110) plane for cold rolling and recrystallization of BCC metals are shown in Fig. 6, which includes the main components of the uniaxial γ-fiber texture: $\{1\bar{1}1\}$ <110> and $\{11\bar{1}\}$ <112> [37-38].

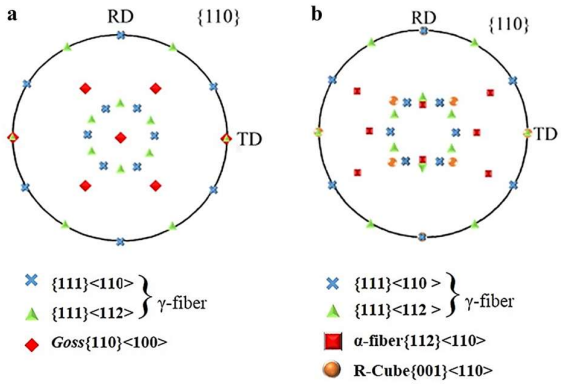

Fig. 6. Position of ideal components and polar image of the plane (110) for common texture in (a) recrystallization, (b) cold rolling of BCC metals [37].

Pole figures of (110) plane for HSLA specimens are shown in Fig. 7, which include pole figure of base metal (Fig. 7(a)), pole figure following the GTAW (Fig. 7(b)), and pole figure after SMAW (Fig. 7(c)). By comparing the ideal pole figure of Fig. 6 and the obtained one in Fig. 7, it can be observed that the texture components related to the recrystallization are developed in the base metal. This texture includes γ-fiber component with orientations of {111} <110> and {111} <112>, and low percentage of α-fiber {112} <110> component. Furthermore, a maximum intensity of 38.5 is observed in the Gauss {110} <001> component, and a minimum intensity of 3.2 is occurred for R-Cube {001} <110> component.

For the GTAW specimen, the intensity and percentage of fibrous components, γ and α, are decreased. The maximum intensity of 26.2 for Gauss components in GTAW has been reduced compared to the base metal and the SMAW specimen, which indicates that a more random texture has been developed. Moreover, the percentage of the R-Cube component in the GTAW specimen is lower than the base metal.

Considering the pole figures of the HSLA specimen after SMAW welding, there is a decrease in the intensity and a higher percentage of the γ-fiber component compared to the GTAW specimen. In SMAW specimen, γ-fiber component has the highest percentage, and the maximum intensity of 46.5 is related to the Gauss component which is higher than the GTAW and even the base metal. However, the Gauss component in the SMAW

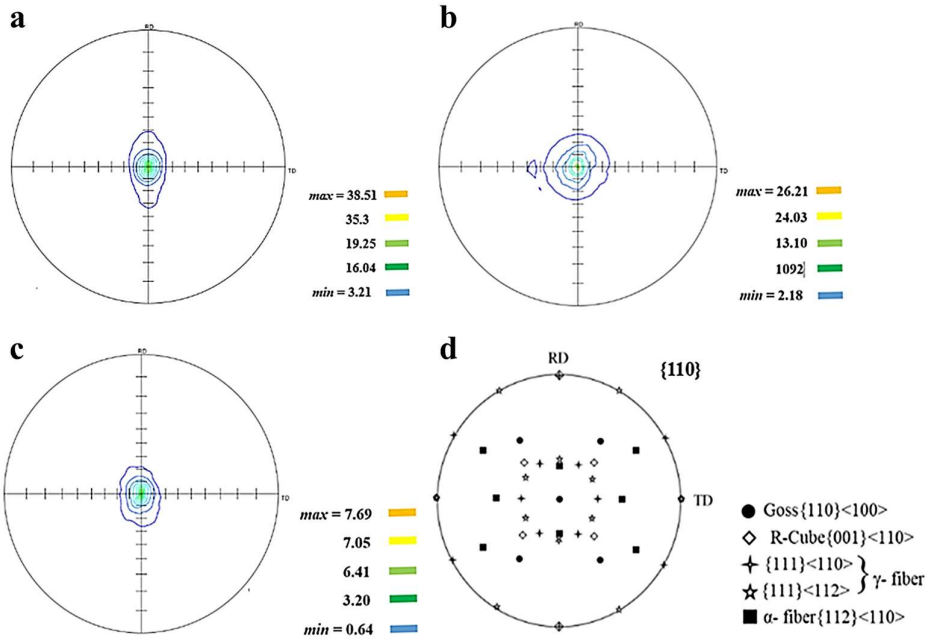

Fig.7. Pole figure of (110) plane for HSLA specimens, (a) base metal specimen before welding, (b) after GTAW, (c) after SMAW, and (d) schematic of the ideal position of common texture components in BCC metals.

specimen is lower than the GTAW specimen. Moreover, the percentage of the R-Cube component in the SMAW is reduced in comparison with the base metal, but is higher than that of the GTAW specimen.

It is widely accepted that the increase in ductility depends on the high percentage of γ-fiber component and a low percentage of the α-fiber [39]. Therefore, by weakening the γ-fiber texture component in welding specimens of SMAW, a drop in the ductility and mechanical properties is expected.

3.3. Hardness variations

The different shape and size of the grains in the weld penetration zone and the HAZ leads to differences in properties such as hardness of the weld bonding areas. Fig. 8 shows micro hardness profile of the weld cross-section of the HSLA specimen welded by SMAW. As can be seen, the hardness of the specimen is not uniform, and by progressing from the base metal towards the center of the weld (Fig. 8-top) the hardness increases and a maximum hardness of 223 Vickers is observed at the weld center. The average hardness of the base metal is 196 Vickers, and in the thickness direction (Fig. 8-bottom) the average hardness is 191 Vickers. The

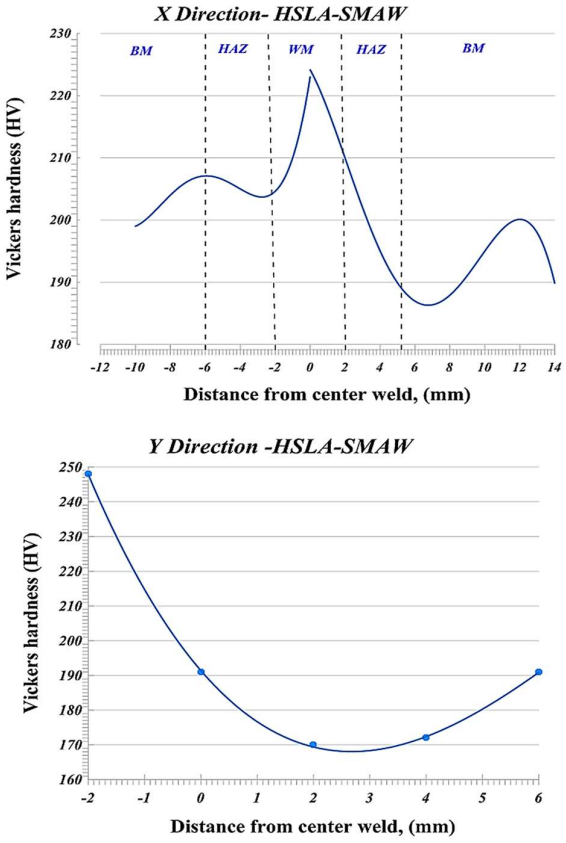

Fig. 8. Hardness profile of weld areas of HSLA specimen welded by SMAW in the direction of length and in the direction of thickness (weld pollen and weld root).

hardness is reduced from the weld pollen to the center of the weld, and at the root of the weld the hardness reaches its maximum value of 248 Vickers.

Fig. 9 shows the micro hardness profile of the HSLA specimen welded by the GTAW method. Along the length of the specimen (Fig. 9-top), as the welding center approaches, the amount of hardness increases and reaches a maximum of 214 Vickers at the center of the weld. In terms of thickness (Fig. 9-bottom), the maximum hardness of the specimen in welding pollen is 261 Vickers. The hardness of the specimen is reduced from the weld pollen to the center of the weld, and then the hardness at the root of the weld reaches 232 Vickers. Having compared the hardness diagrams, it can be confirmed that the amplitude, as well as the stiffness of the HAZ region, in the SMAW welding specimen is greater than the GTAW specimen.

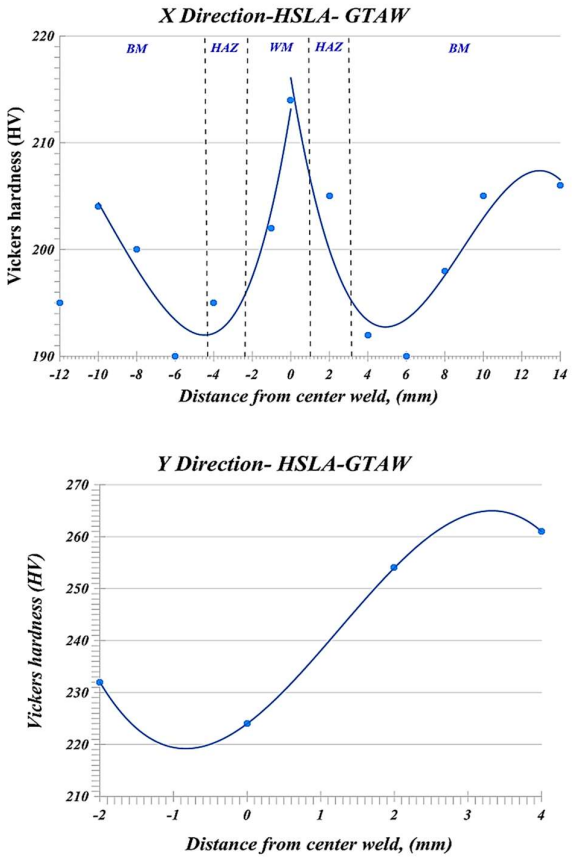

Fig. 9. Hardness profile of weld joints of HSLA specimen welded by GTAW method in the direction of length and in the direction of thickness (weld pollen and weld root).

3.4. Tensile test results

In order to investigate the effect of welding processes on the strength and ductility of specimens, a uniaxial tensile test was performed in three directions of 0, 45, and 90° relative to the welding line. Fig. 10 shows the engineering stress- strain curve of specimens welded by different processes. The amount of elongation and tensile strength is dependent on the direction of welding. Moreover, failure occurred in the weld zone, which indicates that the mechanical properties of the weld cross

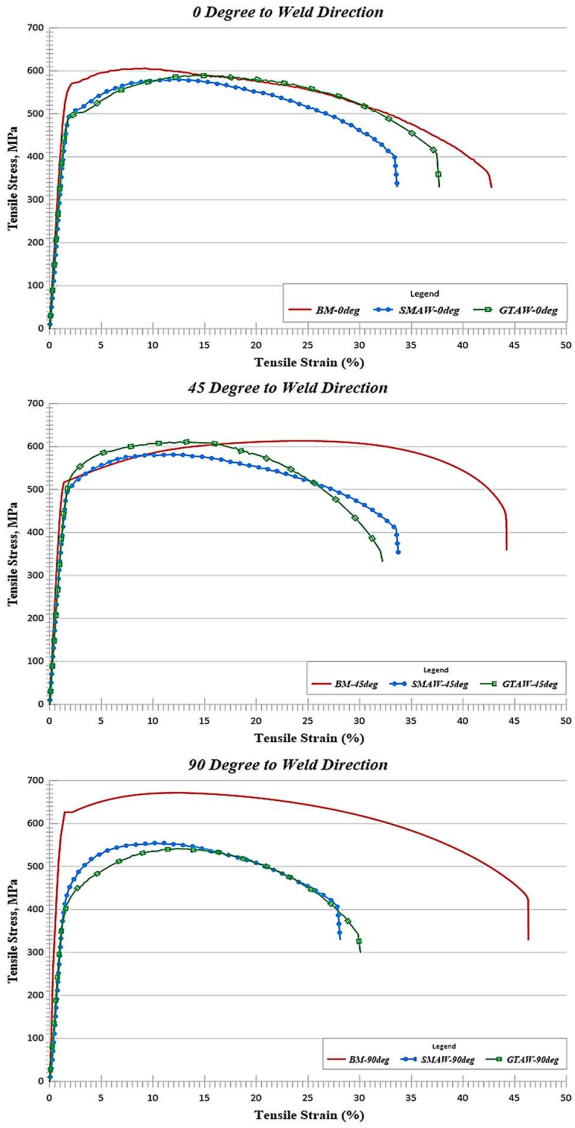

Fig. 10. Engineering stress-strain curve of welding specimens and the base metal in the direction of the weld line, perpendicular to the weld line, and at an angle of 45° to the weld line.

section have decreased compared to the base metal in all types of welding. The greatest decrease in the properties of welded specimens compared to the base metal is observed in the direction perpendicular to that of the welding.

Considering GTAW specimens in the direction of 0 and 45° relative to the welding line, the amount of the tensile strength is higher than the base metal. For 0 and 90° specimens, the percentage of the elongation is greater than the SMAW specimens, which is due to the formation of a narrow HAZ region and fine grain size in the welding areas of GTAW specimens.

Fig. 11 shows the curves of variations in the tensile and yield strengths, and the percentage of elongation of the specimens in terms of angle to the welding direction. The tensile strength, as well as the percentage of the elongation of specimens, are dependent on the angle to the welding direction for different welding methods.

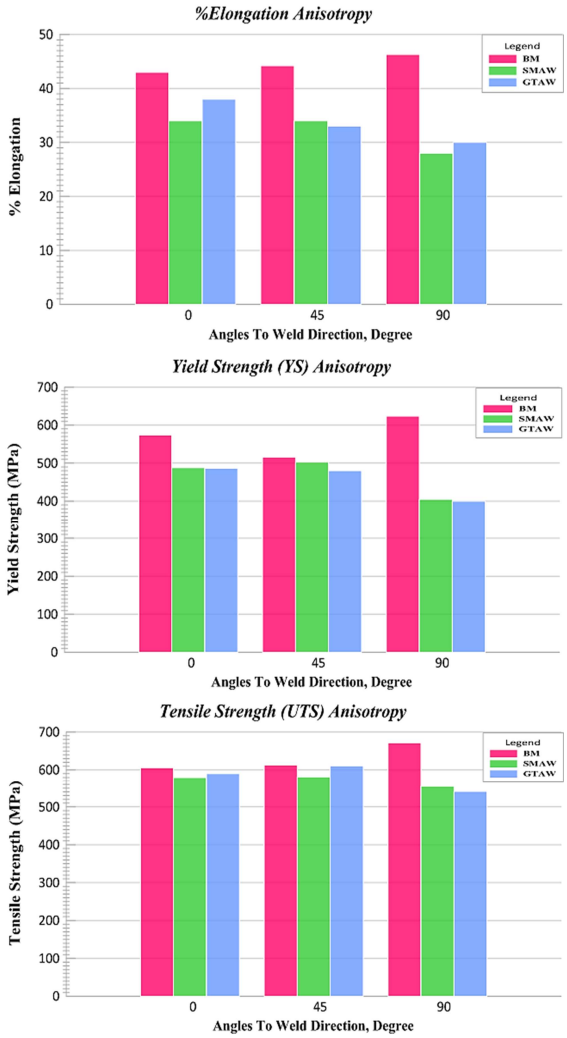

Fig. 11. Percent elongation, yield strength and tensile strength of welding specimens and the base metal in the direction of the weld line, perpendicular to the weld line, and at an angle of 45° to the weld line.

3.5. Anisotropy parameter (r)

Plastic anisotropy parameter (r) was measured by the tensile tests up to the strain of 20% in three directions of 0, 45 and 90° relative to the weld line. The plastic strain ratio r was calculated using the following equation:

$$r = \frac{\varepsilon_w}{\varepsilon_t} \quad (1)$$

where ε_w is the true strain of the specimen in the direction of the width, and ε_t is the true strain in the direction of the thickness of the specimen. As the thickness is difficult to measure due to small variations, the value of r can be obtained from the following equation:

$$r = -\frac{\varepsilon_w}{\varepsilon_L + \varepsilon_w} \quad (2)$$

If r = 1, the sample has the same behavior in both width and thickness; however, increasing the value of r indicates a better ductility [40-42].

Fig. 12 shows the variations of the anisotropy coefficient (r) with θ (angle to the welding direction) for welding specimens. As can be seen, the anisotropy parameters are significantly different in different directions, indicating the anisotropy of the weldment and the base metal. It is evident that the value of the parameter r in all directions is higher in the GTAW welding specimen.

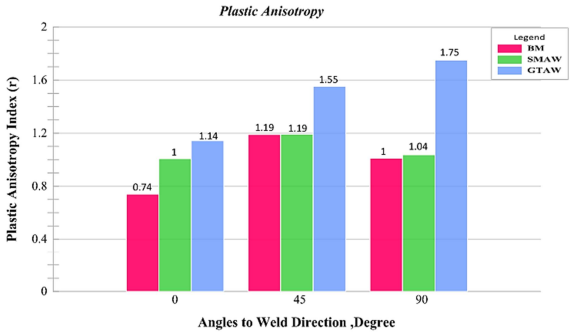

Fig. 12. Variations of the plastic anisotropy coefficient (r value) with θ for welding specimens.

In addition to the anisotropy in the thickness direction, there is also the possibility of anisotropy in the specimen plane. This means that different directions on the specimen have different mechanical behaviors. Therefore, the value of r for the anisotropic metals changes by changing the direction. In this case, the mean value of the anisotropy parameter, normal anisotropy, is defined as follows:

$$R_m = \frac{R_0 + 2R_{45} + R_{90}}{4} \quad (3)$$

where the numbers 0, 45 and 90 indicate the direction of specimen preparation with respect to the direction of the rolling or the direction of the welding line. Planar anisotropy is another indicator of the anisotropy that is mostly used to evaluate the plastic anisotropy of sheets:

$$\Delta R = \frac{R_0 - 2R_{45} + R_{90}}{2} \quad (4)$$

Hot rolled steels are usually isotropic, $R_m = 1$. Increasing the normal anisotropy parameter will increase the deep drawing capability. It is generally accepted that the highest value of R_m and the lowest value of ΔR indicates a better formability [43].

Fig. 13 shows the calculated values of the normal anisotropy and the planar anisotropy parameter for different specimens. The specimens obtained from the GTAW welding have the highest amount of R_m and the lowest ΔR which indicates superior ductility of specimens obtained from the GTAW.

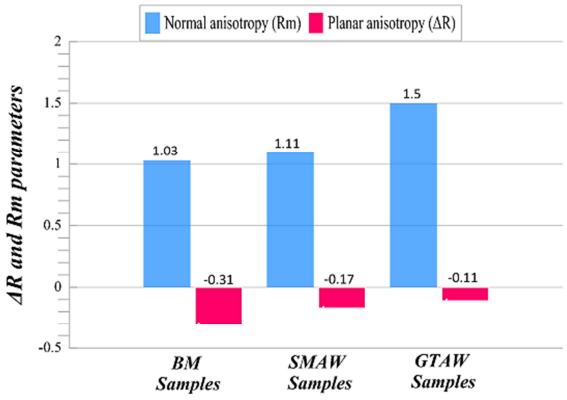

Fig. 13. Effect of welding processes on the values of normal anisotropy parameter (R_m) and planar anisotropy parameter (ΔR).

4. Conclusion

In the present study, the effect of GTAW and SMAW welding processes on the variations in the crystallographic texture and mechanical properties of HSLA steel were investigated. Some of the most important results are as follows:

- Welding processes performed on the specimens cause a change in the intensity and percentage of the primary texture components of the specimens; and as a result, secondary solidification texture with characteristics similar to the primary texture is formed. Welding processes have a significant effect on the texture evolutions and reduce the percentage and intensity of the γ-fiber texture component.
- Concerning GTAW specimens, the rapid solidification due to the high thermal gradient, results in more acicular ferrites and better resistance to the crack propagation. The smaller HAZ area and finer microstructure of GTAW results in superior mechanical properties in comparison with the SMAW specimens.
- The value of the normal anisotropy parameter in the base metal was approximately equal to 1, which indicates the isotropy of the mechanical properties. In contrast, due to the GTAW process, the value of the normal anisotropy increased, which indicates an increase of the anisotropy in terms of mechanical properties. The amount of normal anisotropy in the SMAW specimen is close to the base metal, which indicates that these specimens are more isotropic than the GTAW ones.
- Considering the results of the tensile test and texture evaluations, it can be concluded that the weakening of the γ-fiber texture component in the welded specimens significantly decreases its ductility and mechanical properties.

Acknowledgment

The authors wish to thanks materials processing labaratory of KN Toosi University of Technology for providing facilities for part of experiments.

Funding

This research had not received any funds.

Conflict of Interests

The authors declare that they have no known competing financial interests or personal relationships that could have appeared to influence the work reported in this paper.

5. References

[1] S.R. Nathan, V. Balasubramanian, S. Malarvizhi, A.G. Rao, Effect of welding processes on mechanical and microstructural characteristics of high strength low alloy naval grade steel joints, *Defence Technology*, 11(3) (2015) 308-317.

[2] D.A. Skobir, High-strength low-alloy (HSLA) steels, *Materials and Technology*, 45(4) (2011) 295-301.

[3] Z. Jia, R.D.K. Misra, R. O'malley, S.J. Jansto, Fine-scale precipitation and mechanical properties of thin slab processed titanium-niobium bearing high strength steels, *Materials Science and Engineering: A*, 528(22–23) (2011) 7077-7083.

[4] S.K. Dhua, D. Mukerjee, D.S. Sarma, Influence of tempering on the microstructure and mechanical properties of HSLA-100 steel plates, *Metallurgical and Materials Transactions A*, 32(9) (2001) 2259-2270.

[5] P. Hariprasath, P. Sivaraj, V. Balasubramanian, S. Pilli, K. Sridhar, Effect of the welding technique on mechanical properties and metallurgical characteristics of the naval grade high strength low alloy steel joints produced by SMAW and GMAW, *CIRP Journal of Manufacturing Science and Technology*, 37 (2022) 584-595.

[6] T.B. Hilditch, T. De Souza, P.D. Hodgson, Properties and automotive applications of Advanced High-Strength Steels (AHSS), In Welding and joining of advanced high strength steels (AHSS), Woodhead Publishing, 2015, pp. 9-28.

[7] N.J. Den Uijl, L.J. Carless, Advanced metal-forming technologies for automotive applications, In Advanced materials in automotive engineering, Woodhead Publishing, 2012, pp. 28-56.

[8] S.G. Jansto, Niobium-bearing steel development for value-added structural applications, New developments on metallurgy and applications of high strength steels; TMS: Warrendale, PA, USA, 2008, pp. 1313-1326.

[9] K.K. Ramachandran, N. Murugan, S.S. Kumar, Effect of tool axis offset and geometry of tool pin profile on the characteristics of friction stir welded dissimilar joints of aluminum alloy AA5052 and HSLA steel, *Materials Science and Engineering: A*, 639 (2015) 219-233.

[10] S. Vervynckt, K. Erbeken, B. Lopez, J.J. Jonas, Modern HSLA steels and role of non-recrystallisation temperature, *International Materials Reviews*, 57(4) (2012) 187-207.

[11] Y. Liu, L. Shi, C. Liu, L. Yu, Z. Yan, H. Li, Effect of step quenching on microstructures and mechanical properties of HSLA steel, *Materials Science and Engineering: A*, 675 (2016) 371-378.

[12] H.J. Kong, C. Xu, C.C. Bu, C. Da, J.H. Luan, Z.B. Jiao, G. Chen, C.T. Liu, Hardening mechanisms and impact toughening of a high-strength steel containing low Ni and Cu additions, *Acta Materialia*, 172 (2019) 150-160.

[13] Q. Fang, L. Zhao, B. Liu, C. Chen, Y. Peng, Z. Tian, F. Yin, Microstructure and mechanical properties of 800-MPa-class high-strength low-alloy steel part fabricated by wire arc additive manufacturing, *Journal of Materials Engineering and Performance*, 31 (2022) 7461-7471.

[14] K. Kornokar, F. Nematzadeh, H. Mostaan, A. Sadeghian, M. Moradi, D.G. Waugh, M. Bodaghi, Influence of heat input on microstructure and mechanical properties of gastungsten arc welded HSLA S500MC steel joints, *Metals*, 12(4) (2022) 565.

[15] M.H.A Musa, M.A. Maleque, M.Y. Ali, An investigation of TIG welding parameters on microhardness and microstructure of heat affected zone of HSLA steel, *Materials Science and Engineering*, 290(1) (2018) 012041.

[16] M. Mukherjee, T.K. Pal, Influence of mode of metal transfer on microstructure and mechanical properties of gas metal arc-welded modified ferritic stainless steel, *Metallurgical and Materials Transactions A*, 43(6) (2012) 1791-1808.

[17] L.G. Hector, Y.L. Chen, S. Agarwal, C.L. Briant, Texture characterization of autogenous Nd: YAG laser welds in AA5182-O and AA6111-T4 aluminum alloys, *Metallurgical and Materials Transactions A*, 35(9) (2004) 3032-3038.

[18] M. Venkateshkannan, N. Arivazhagan, M. Nageswara Rao, G. Madhusudhan Reddy, Characterization of weld joints produced by continuous wave and double pulse gas metal arc welding in naval grade high-strength low-alloy steel, *Proceedings of the Institution of Mechanical*

Engineers, Part E: Journal of Process Mechanical Engineering, (2022) 09544089221126430.

[19] A.K. Perka, M. John, U.B. Kuruveri, P.L. Menezes, Advanced high-strength steels for automotive applications: arc and laser welding process, properties, and challenges, *Metals*, 12(6) (2022) 1051.

[20] F.F. Chen, J. Xiang, D.G. Thomas, A.B. Murphy, Model-based parameter optimization for arc welding process simulation, *Applied Mathematical Modelling*, 81 (2020) 386-400.

[21] S.P. Tewari, A. Gupta, J. Prakash, Effect of welding parameters on the weldability of material, *International Journal of Engineering Science and Technology*, 2(4) (2010) 512-516.

[22] S.I.A. Talabi, O.B.B. Owolabi, J.A.A. Adebisi, Effect of welding variables on mechanical properties of low carbon steel welded joint, *Advances in Production Engineering & Management*, 9(4) (2014) 181-186.

[23] D. Simhachalam, M.S.S. Rao, B.N. Raju, Evaluation of mechanical properties of stainless steel (ss 304) by tig welding at heat affected zone, *International Journal of Engineering and Management Research (IJEMR)*, 5(4) (2015) 214-221.

[24] R. Lal, M. Shuaib, V. Paliwal, Comparative study of mechanical properties of TIG welded joints of similar and dissimilar grades of Stainless Steel material, *International Journal of Advance Research and Innovation*, 6(3) (2018) 205-208.

[25] J. Yan, M. Gao, X. Zeng, Study on microstructure and mechanical properties of 304 stainless steel joints by TIG, laser and laser-TIG hybrid welding, *Optics and Lasers in Engineering*, 48(4) (2010) 512-517.

[26] S. Saha, M. Mukherjee, T.K. Pal, Microstructure, texture, and mechanical property analysis of gas metal arc welded AISI 304 austenitic stainless steel, *Journal of Materials Engineering and Performance*, 24(3) (2014) 1125-1139.

[27] P. Yan, Ö.E. Güngör, P. Thibaux, H.K. Bhadeshia, Crystallographic texture of induction-welded and heat-treated pipeline steel, *Advanced Materials Research*, 89 (2010) 651-656.

[28] M. Gustafsson, M. Thuvander, E.L. Bergqvist, E. Keehan, L. Karlsson, Effect of welding procedure on texture and strength of nickel based weld metal, *Science and Technology of Welding and Joining*, 12(6) (2007) 549-555.

[29] L. Wang, P. Zhou, Y. Hu, B. Wang, Effect of microstructure and texture on the mechanical properties in high strength pipeline bend, *International Journal of Pressure Vessels and Piping*, 195 (2022) 104604.

[30] Technical handbook of Bohler welding products, 8605 Kapfenberg/Austria, 2005.

[31] K. Kumar, A. Pooleery, K. Madhusoodanan, R.N. Singh, J.K. Chakravartty, B.K. Dutta, R.K. Sinha, Use of miniature tensile specimen for measurement of mechanical properties, *Procedia Engineering*, 86 (2014) 899-909.

[32] H.K. Bhadeshia, Strong ferritic-steel welds, *Materials Science Forum*, 539 (2007) 6-11.

[33] P.G. Jonsson, A.B. Murphy, J. Szekely, The influence of oxygen additions on argon-shielded gas metal arc welding processes, *Welding Research Supplement*, 74(2) (1995) 48-57.

[34] C.H. Lee, H.K.D.H. Bhadeshia, H.C. Lee, Effect of plastic deformation on the formation of accicular ferrite, *Materials Science Engineering: A*, 360 (1-2) (2003) 249-257.

[35] P.A.Ş.A. Yayla, E. Kaluc, K. Ural, Effects of welding processes on the mechanical properties of HY 80 steel weldments, *Materials & Design*, 28(6) (2007) 1898-1906.

[36] W. Sun, G. Wang, J. Zhang, D. Xia, H. Sun, Microstructure characterization of high-heat-input welding joint of HSLA steel plate for oil storage construction, *Journal of Materials Science & Technology*, 25(6) (2009) 857.

[37] L. Seidel, M. Hölscher, K. Lücke, Rolling and recrystallization textures in iron-3% silicon, *Texture and Microstructure*, 11(2-4) (1989) 171-185.

[38] A.A. Vasilyev, N.Y. Zolotorevsky, D.F. Sokolov, S.A. Philippov, Crystallographic texture of industrial automotive steels and effect of tertiary cementite dissolution on its development, *Materials Physics & Mechanics*, 47(3) (2021) 399-407.

[39] R.K. Ray, J.J. Jonas, R.E. Hook, Cold rolling and annealing texture in low carbon and extra low carbon steels, *International Materials Reviews*, 39(4) (1994) 129-172.

[40] R.K. Ray, P. Ghosh, Texture in the design of advanced steels, *Transactions of the Indian Institute of Metals*, 66(5) (2013) 641-653.

[41] S. Hoile, Processing and properties of mild interstitial free steels, *Materials Science and Technology*, 16(10) (2000) 1079-1093.

[42] T. Ogawa, Y. Suzuki, Y. Adachi, A. Yamaguchi, Y. Matsubara, Effect of cold-rolling directions on recrystallization texture, *Materials*, 15(9) (2022) 3083.

[43] N.D.A. Sardinha, I.C.D. Santos, B.V. Andrade, R.A. Botelho, R.V.D. Oliveria, S.B. Diniz, A.D.S. Paula, Mechanical properties and crystallographic texture of symmetrical and asymmetrical cold rolled IF steels, *Materials Research*, 19(5) (2016) 1042-1048.